

# Phase anomalies in Bessel-Gauss beams

Myun-Sik Kim,<sup>1,\*</sup> Toralf Scharf,<sup>1</sup> Alberto da Costa Assafrao,<sup>2</sup> Carsten Rockstuhl,<sup>3</sup> Sylvania F. Pereira,<sup>2</sup> H. Paul Urbach,<sup>2</sup> and Hans Peter Herzig<sup>1</sup>

<sup>1</sup>Optics & Photonics Technology Laboratory, Ecole Polytechnique Fédérale de Lausanne (EPFL), Neuchâtel, CH-2000, Switzerland

<sup>2</sup>Optics Research Group, Delft University of Technology, Lorentzweg 1, 2628 CJ Delft, The Netherlands

<sup>3</sup>Institute of Condensed Matter Theory and Solid State Optics, Abbe Center of Photonics, Friedrich-Schiller-Universität Jena, 07743 Jena, Germany

\*myunsik.kim@epfl.ch

**Abstract:** Bessel-Gauss beams are known as non-diffracting beams. They can be obtained by focusing an annularly shaped collimated laser beam. Here, we report for the first time on the direct measurement of the phase evolution of such beams by relying on longitudinal-differential interferometry. We found that the characteristics of Bessel-Gauss beams cause a continuously increasing phase anomaly in the spatial domain where such beams do not diverge, i.e. there is a larger phase advance of the beam when compared to a referential plane wave. Simulations are in excellent agreement with measurements. We also provide an analytical treatment of the problem that matches both experimental and numerical results and provides an intuitive explanation.

©2012 Optical Society of America

OCIS codes: (050.5080) Phase shift; (100.5088) Phase unwrapping; (260.0260) Physical optics; (260.6042) Singular optics; (180.3170) Interference microscopy.

---

## References and links

1. L. G. Gouy, "Sur une propriété nouvelle des ondes lumineuses," *C. R. Acad. Sci.* **110**, 1251–1253 (1890).
2. A. E. Siegman, *Lasers* (University Science Books, 1986).
3. M. Born and E. Wolf, *Principles of Optics*, 7th ed (Cambridge University Press, 1999).
4. F. Gittes and C. F. Schmidt, "Interference model for back-focal-plane displacement detection in optical tweezers," *Opt. Lett.* **23**(1), 7–9 (1998).
5. B. Roy, S. B. Pal, A. Haldar, R. K. Gupta, N. Ghosh, and A. Banerjee, "Probing the dynamics of an optically trapped particle by phase sensitive back focal plane interferometry," *Opt. Express* **20**(8), 8317–8328 (2012).
6. L. Friedrich and A. Rohrbach, "Tuning the detection sensitivity: a model for axial backfocal plane interferometric tracking," *Opt. Lett.* **37**(11), 2109–2111 (2012).
7. R. W. Boyd, *Nonlinear Optics*, 2nd ed. (Academic Press, San Diego, 1992)
8. S. Carrasco, B. E. A. Saleh, M. C. Teich, and J. T. Fourkas, "Second- and third-harmonic generation with vector Gaussian beams," *J. Opt. Soc. Am. B* **23**(10), 2134–2141 (2006).
9. C. Zhang, Y.-Q. Qin, and Y.-Y. Zhu, "Perfect quasi-phase matching for the third-harmonic generation using focused Gaussian beams," *Opt. Lett.* **33**(7), 720–722 (2008).
10. T. Popmintchev, M.-C. Chen, P. Arpin, M. M. Murnane, and H. C. Kapteyn, "The attosecond nonlinear optics of bright coherent X-ray generation," *Nat. Photonics* **4**(12), 822–832 (2010).
11. J. T. Foley and E. Wolf, "Wave-front spacing in the focal region of high-numerical-aperture systems," *Opt. Lett.* **30**(11), 1312–1314 (2005).
12. H. Chen, Q. Zhan, Y. Zhang, and Y.-P. Li, "The Gouy phase shift of the highly focused radially polarized beam," *Phys. Lett. A* **371**(3), 259–261 (2007).
13. T. Tyc, "Gouy phase for full-aperture spherical and cylindrical waves," *Opt. Lett.* **37**(5), 924–926 (2012).
14. R. W. Boyd, "Intuitive explanation of the phase anomaly of focused light beams," *J. Opt. Soc. Am.* **70**(7), 877–880 (1980).
15. D. Subbarao, "Topological phase in Gaussian beam optics," *Opt. Lett.* **20**(21), 2162–2164 (1995).
16. R. Simon and N. Mukunda, "Bargmann invariant and the geometry of the Gouy effect," *Phys. Rev. Lett.* **70**(7), 880–883 (1993).
17. S. J. M. Habraken and G. Nienhuis, "Geometric phases in astigmatic optical modes of arbitrary order," *J. Math. Phys.* **51**(8), 082702 (2010).
18. G. F. Brand, "A new millimeter wave geometric phase demonstration," *Int. J. Infrared Millim. Waves* **21**(4), 505–518 (2000).
19. P. Hariharan and P. A. Robinson, "The Gouy phase shift as a geometrical quantum effect," *J. Mod. Opt.* **43**, 219–221 (1996).
20. S. Feng and H. G. Winful, "Physical origin of the Gouy phase shift," *Opt. Lett.* **26**(8), 485–487 (2001).

21. I. G. da Paz, P. L. Saldanha, M. C. Nemes, and J. G. Peixoto de Faria, "Experimental proposal for measuring the Gouy phase of matter waves," *New J. Phys.* **13**(12), 125005 (2011).
22. T. D. Visser and E. Wolf, "The origin of the Gouy phase anomaly and its generalization to astigmatic wavefields," *Opt. Commun.* **283**(18), 3371–3375 (2010).
23. J. P. Rolland, K. P. Thompson, K.-S. Lee, J. Tamkin, Jr., T. Schmid, and E. Wolf, "Observation of the Gouy phase anomaly in astigmatic beams," *Appl. Opt.* **51**(15), 2902–2908 (2012).
24. N. C. R. Holme, B. C. Daly, M. T. Myaing, and T. B. Norris, "Gouy phase shift of single-cycle picosecond acoustic pulses," *Appl. Phys. Lett.* **83**(2), 392–394 (2003).
25. C. R. Carpenter, "Gouy phase advance with microwaves," *Am. J. Phys.* **27**, 98–100 (1959).
26. J. F. Federici, R. L. Wample, D. Rodriguez, and S. Mukherjee, "Application of terahertz Gouy phase shift from curved surfaces for estimation of crop yield," *Appl. Opt.* **48**(7), 1382–1388 (2009).
27. A. B. Ruffin, J. V. Rudd, J. F. Whitaker, S. Feng, and H. G. Winful, "Direct observation of the Gouy phase shift with single-cycle terahertz pulse," *Phys. Rev. Lett.* **83**(17), 3410–3413 (1999).
28. H. He and X.-C. Zhang, "Analysis of Gouy phase shift for optimizing terahertz air-biased-coherent-detection," *Appl. Phys. Lett.* **100**(6), 061105 (2012).
29. B. E. A. Saleh and M. C. Teich, *Fundamentals of Photonics* (Wiley, New York, 1991).
30. H. Kogelnik and T. Li, "Laser beams and resonators," *Appl. Opt.* **5**(10), 1550–1567 (1966).
31. T. Ackemanna, W. Grosse-Nobis, and G. L. Lippia, "The Gouy phase shift, the average phase lag of Fourier components of Hermite-Gaussian modes and their application to resonance conditions in optical cavities," *Opt. Commun.* **189**(1-3), 5–14 (2001).
32. J. Courtial, "Self-imaging beams and the Guoy effect," *Opt. Commun.* **151**(1-3), 1–4 (1998).
33. J. Hamazaki, Y. Mineta, K. Oka, and R. Morita, "Direct observation of Gouy phase shift in a propagating optical vortex," *Opt. Express* **14**(18), 8382–8392 (2006).
34. H. X. Cui, X. L. Wang, B. Gu, Y. N. Li, J. Chen, and H. T. Wang, "Angular diffraction of an optical vortex induced by the Gouy phase," *J. Opt.* **14**(5), 055707 (2012).
35. X. Pang, G. Gbur, and T. D. Visser, "The Gouy phase of Airy beams," *Opt. Lett.* **36**(13), 2492–2494 (2011).
36. R. Gadonas, V. Jarutis, R. Paškauskas, V. Smilgevičius, A. Stabinis, and V. Vaičaitis, "Self-action of Bessel beam in nonlinear medium," *Opt. Commun.* **196**(1-6), 309–316 (2001).
37. P. Martelli, M. Tacca, A. Gatto, G. Moneta, and M. Martinelli, "Gouy phase shift in nondiffracting Bessel beams," *Opt. Express* **18**(7), 7108–7120 (2010).
38. W. Zhu, A. Agrawal, and A. Nahata, "Direct measurement of the Gouy phase shift for surface plasmon-polaritons," *Opt. Express* **15**(16), 9995–10001 (2007).
39. M.-S. Kim, T. Scharf, S. Mühlig, C. Rockstuhl, and H. P. Herzig, "Gouy phase anomaly in photonic nanojets," *Appl. Phys. Lett.* **98**(19), 191114 (2011).
40. M.-S. Kim, T. Scharf, C. Etrich, C. Rockstuhl, and H. H. Peter, "Longitudinal-differential interferometry: Direct imaging of axial superluminal phase propagation," *Opt. Lett.* **37**(3), 305–307 (2012).
41. D. Chauvat, O. Emile, M. Brunel, and A. Le Floch, "Direct measurement of the central fringe velocity in Young-type experiments," *Phys. Lett. A* **295**(2-3), 78–80 (2002).
42. M. Vasnetsov, V. Pas'ko, A. Khoroshun, V. Slyusar, and M. Soskin, "Observation of superluminal wave-front propagation at the shadow area behind an opaque disk," *Opt. Lett.* **32**(13), 1830–1832 (2007).
43. Q. Zhan, "Second-order tilted wave interpretation of the Gouy phase shift under high numerical aperture uniform illumination," *Opt. Commun.* **242**(4-6), 351–360 (2004).
44. F. O. Fahrbach, P. Simon, and A. Rohrbach, "Microscopy with self-reconstructing beams," *Nat. Photonics* **4**(11), 780–785 (2010).
45. F. O. Fahrbach and A. Rohrbach, "Propagation stability of self-reconstructing Bessel beams enables contrast-enhanced imaging in thick media," *Nat Commun* **3**, 632 (2012).
46. T. A. Planchon, L. Gao, D. E. Milkie, M. W. Davidson, J. A. Galbraith, C. G. Galbraith, and E. Betzig, "Rapid three-dimensional isotropic imaging of living cells using Bessel beam plane illumination," *Nat. Methods* **8**(5), 417–423 (2011).
47. B. Sick, B. Hecht, and L. Novotny, "Orientational imaging of single molecules by annular illumination," *Phys. Rev. Lett.* **85**(21), 4482–4485 (2000).
48. V. Garcés-Chávez, D. McGloin, H. Melville, W. Sibbett, and K. Dholakia, "Simultaneous micromanipulation in multiple planes using a self-reconstructing light beam," *Nature* **419**(6903), 145–147 (2002).
49. E. McLeod and C. B. Arnold, "Subwavelength direct-write nanopatterning using optically trapped microspheres," *Nat. Nanotechnol.* **3**(7), 413–417 (2008).
50. J. Arlt, V. Garcés-Chavez, W. Sibbett, and K. Dholakia, "Optical micromanipulation using a Bessel light beam," *Opt. Commun.* **197**(4-6), 239–245 (2001).
51. V. Garcés-Chávez, D. McGloin, M. J. Padgett, W. Dultz, H. Schmitzer, and K. Dholakia, "Observation of the transfer of the local angular momentum density of a multiringed light beam to an optically trapped particle," *Phys. Rev. Lett.* **91**(9), 093602 (2003).
52. M. K. Bhuyan, F. Courvoisier, P.-A. Lacourt, M. Jacquot, L. Furfaro, M. J. Withford, and J. M. Dudley, "High aspect ratio taper-free microchannel fabrication using femtosecond Bessel beams," *Opt. Express* **18**(2), 566–574 (2010).
53. X.-F. Li, R. J. Winfield, S. O'Brien, and G. M. Crean, "Application of Bessel beams to 2D microfabrication," *Appl. Surf. Sci.* **255**(10), 5146–5149 (2009).
54. H. Wang, L. Shi, B. Lukyanchuk, C. Sheppard, and C. T. Chong, "Creation of a needle of longitudinally polarized light in vacuum using binary optics," *Nat. Photonics* **2**(8), 501–505 (2008).

55. B. Richards and E. Wolf, "Electromagnetic diffraction in optical systems. II. Structure of the image field in an aplanatic system," *Proc. R. Soc. Lond. A Math. Phys. Sci.* **253**(1274), 358–379 (1959).
  56. J. Durmin, J. J. Miceli, Jr., and J. H. Eberly, "Diffraction-free beams," *Phys. Rev. Lett.* **58**(15), 1499–1501 (1987).
  57. F. Gori, G. Guattari, and C. Padovani, "Bessel-Gauss beams," *Opt. Commun.* **64**(6), 491–495 (1987).
  58. J. H. McLeod, "The axicon: A new type of optical element," *J. Opt. Soc. Am.* **44**(8), 592–597 (1954).
  59. G. Indebetouw, "Nondiffracting optical fields: some remarks in their analysis and synthesis," *J. Opt. Soc. Am. A* **6**(1), 150–152 (1989).
  60. A. Vasara, J. Turunen, and A. T. Friberg, "Realization of general nondiffracting beams with computer-generated holograms," *J. Opt. Soc. Am. A* **6**(11), 1748–1754 (1989).
  61. Q. Huang, S. Coetmellec, F. Duval, A. Louis, H. Leblond, and M. Brunel, "Analytical expressions for diffraction-free beams through an opaque disk," *J. Europ. Opt. Soc. Rap. Public.* **6**, 11031 (2011).
  62. C. J. R. Sheppard and T. Wilson, "Gaussian-beam theory of lenses with annular aperture," *IEEE J. Microwaves, Opt. Acoust.* **2**(4), 105–112 (1978).
  63. M.-S. Kim, T. Scharf, S. Mühlig, C. Rockstuhl, and H. P. Herzig, "Engineering photonic nanojets," *Opt. Express* **19**(11), 10206–10220 (2011).
  64. M.-S. Kim, T. Scharf, and H. P. Herzig, "Small-size microlens characterization by multiwavelength high-resolution interference microscopy," *Opt. Express* **18**(14), 14319–14329 (2010).
  65. X. Pang, D. G. Fischer, and T. D. Visser, "Generalized Gouy phase for focused partially coherent light and its implications for interferometry," *J. Opt. Soc. Am. A* **29**(6), 989–993 (2012).
  66. E. H. Linfoot and E. Wolf, "Phase distribution near focus in an aberration-free diffraction image," *Proc. Phys. Soc. Lond.* **69**(8), 823–832 (1956).
- 

## 1. Introduction

Anomalous axial phase behavior of optical beams has been drawing attention since Gouy's discovery in 1890 [1] and is called after him *Gouy phase* or *phase anomaly*. This peculiar phase behavior plays an essential role in various physical problems and applications thereof. For fundamental physics, first, it intuitively explains the  $\pi/2$  phase shift of the secondary Huygens' wavelets emerging from a primary wavefront [2, 3]. Second, in laser cavities the resonance frequencies of different transverse modes are determined by the Gouy phase [2, 3]. Applied physics problems also rely on it. A prime example are optical trapping schemes where the Gouy phase is at the origin of a lateral trapping force [4] and where it can provide a tracking mechanism of trapped particles [5,6]. Moreover, the generation of higher harmonics employs phase-matching techniques by considering this phase anomaly; not only in nonlinear optics [7–9] but also in attosecond science [10].

Although, Gouy's discovery took place more than hundred years ago, curiosity about the origin and physical meanings of this phenomenon continually induces discussions which are developed from different theoretical perspectives. The wavefront spacing, which is defined as the smallest distance between surfaces of constant phase on which the values differ by  $2\pi$  [11], can demonstrate how such on-axis phase shifts occur in focused waves compared to the plane wave. Note that for monochromatic plane wave fields this wavefront spacing equals the wavelength but it may differ significantly for spatially inhomogeneous wave fields. In this context, both analytical and numerical studies for radially polarized beams have been reported [12]. The 2D and 3D focusing cases have been analyzed applying mathematical techniques that directly demonstrate irregular wavefront spacing [13]. Other theories were considered as well. For example, the geometric properties of Gaussian beams [14], Berry's geometrical phase [15–18], and even quantum mechanics [19–21] have been considered to give more insights. Recently, it has also been explored in the context of deviating wave fields, i.e. astigmatic wave fields [22, 23].

The aim of this study is to investigate the Gouy phase anomaly in non-diffracting Bessel-Gauss beam, where the quantity of the axial phase shift is expected to be distinct from that of the focused fundamental Gaussian beam. We apply experimental and numerical methods, and then an analytical treatment is provided for an intuitive explanation. The remainder of this work is organized as follows. We start with the varieties of occurrences and quantities of the Gouy phase anomalies (section 2) and discuss the non-diffracting Bessel beam and its generation (section 3). In section 4, the details of the experimental theoretical backgrounds are explained. Next, in sections 5 and 6, the intensity and phase distributions of the focused Bessel-Gauss beam are presented, respectively. In section 7, the overall discussions for the

Gouy phase anomalies in the Bessel-Gauss beam follow. The conclusions of this study are given in section 8.

## 2. Various occurrences and quantities of Gouy phase anomalies

In Gouy's original experiment [1], a light diverging from a point source was reflected from a planar and a concave mirror. These two light beams were overlapped to cause circular interference fringes in a plane of observation. The appearance of the central fringe was shifted from dark to bright, or *vice versa*, at observation planes just before or after the focus [see Chapter 17 in Ref. 2]. This change of intensity, demonstrating destructive and constructive interferences, indicates a  $\pi$  shift of the converging wave with respect to the phase of the on-axis plane wave. Gouy's prediction, such as, the occurrence of the effect in any kind of waves, was straightforward and intuitive. As a proof, such phase anomalies have been demonstrated not only in optical waves but also in acoustic waves [24], microwaves [18, 25], and terahertz waves [26–28]. In optical waves, various classes of beams exhibit the Gouy phase, e.g., general higher Gaussian modes like Hermite-Gaussian and Laguerre-Gaussian beams [2, 29–32], more specifically a vortex beam [33, 34], a radially polarized beam [12], the Airy beam [35], and the Bessel beam [36, 37]. In addition to such optical beams, surface plasmon-polaritons [38], matter waves [21], scattered hotspots (i.e. a photonic nanojet) [39], and diffracted hotspots (i.e. the spot of Arago) [40–42] also exhibit axial phase shifts. The amount of such axial phase shifts differs depending on the type of beams and the confinement situations. The exact determination of this amount is of major importance.

In general, the Gouy phase is characterized by  $\alpha\pi/2$  axial phase shift for a converging light wave passing through its focus upon propagation from  $-\infty$  to  $+\infty$ . The factor  $\alpha$  is a dimension-related value, which equals 1 for a line focus representing the two-dimensional (2D) case (i.e. cylindrical wave) and equals 2 for a point focus representing the three-dimensional (3D) case (i.e. spherical wave). By dividing an aberration-free point focus into two regions, i.e. a converging part and a diverging part, the Gouy phase is defined as a cumulative phase shift of  $\pi/2$  on either side of the focus. In other words, one half of the overall phase shift is acquired while passing each spatial domain. This intuitively explains the imaginary factor  $i$  in the Huygens' integral corresponding to a  $\pi/2$  phase shift acquired by the secondary wavelets diverging from each point of the primary incident wavefront [2, 3], in Huygens-Fresnel, Kirchhoff, and Rayleigh-Sommerfeld diffraction integrals as well. When the secondary wavelets emerge from the primary wavefront, they experience only the diverging part. This situation corresponds to only one half of the focusing situation. Consequently, the amount of the phase shift of these secondary wavelets equals half the Gouy phase of a point focus. Another interesting example for the only diverging case is the spot of Arago. In this case the axial phase shift starts with an initial phase lag and decreases proportional to the optical path difference ( $\Delta\text{OPD}$ ) between an incident on-axis plane wave and the diffracted wave emerging from the rim of the circular obstacle [40]. This diffracted wave travels  $(z^2 + r^2)^{1/2}$ , where  $z$  is the distance along the optical axis and  $r$  is the radius of the obstacle. It leads to  $\Delta\text{OPD} = (z^2 + r^2)^{1/2} - z$  and the axial phase shift is  $\Delta\phi = -\Delta\text{OPD} \cdot 2\pi/\lambda$ . Here, the maximum phase difference occurs just behind the obstacle, at  $z = 0$ . It equals  $-r \cdot 2\pi/\lambda$  that is in fact the initial phase lag of an on-axis point in the plane of  $z = 0$ . Upon the diffracted wave propagating to the far field,  $\Delta\phi$  decreases and vanishes for an infinite distance, i.e.  $\Delta\text{OPD} = 0 \rightarrow \Delta\phi = 0$ . An analogy of a focusing situation is the fundamental Gaussian mode, i.e.  $\text{TEM}_{00}$ . The phase shift is given by  $\Delta\phi_G = -\tan^{-1}(z/Z_R)$  with  $Z_R$  = the Rayleigh range, and the maximum amount is  $\pi$  for the case of propagation from  $-\infty$  to  $+\infty$ . The shift within  $\pm Z_R$  is the most prominent and the amount is found to be  $\pi/2$ . Higher modes, i.e. the Hermite-Gaussian and Laguerre-Gaussian modes, demonstrate a larger shift compared to the fundamental mode due to their different resonance frequencies. The Hermite-Gaussian modes exceed the fundamental Gouy phase ( $\Delta\phi_G$ ) by a factor of  $m + n + 1$  ( $m$  and  $n$  are the transverse mode numbers) and the Laguerre-Gaussian modes by a factor of  $2p + l + 1$  ( $p$  and  $l$  are the radial and angular mode numbers) [2, 29]. This is the reason why the Gouy effect

plays a fundamental role in determining the resonant frequencies of the laser cavities [29]. In the case of a photonic nanojet a  $\pi$  phase shift is found due to the 3D light confinement that imitates a focusing mechanism [39]. The amount of the phase shift of a non-diffracting Bessel beam is somewhat different from the general Gouy phase, i.e.  $\pi$  shift. It can be understood by using the tilted wave concept [43], where the phase shift originates from the difference between the original wave vector and its on-axis longitudinal projection.

### 3. Bessel beam and its generation

Bessel beams itself are of major importance. The remarkable features of the Bessel beam are of great interest in applications requiring a large depth of focus and a self-healing capacity, especially for imaging microscopy [44–47], optical manipulations [48–51] or micro- and nano-fabrication [49, 52, 53]. Moreover, increasing demands of the resolution in nano-science pushes the size of Bessel beams down to sub-wavelength range and the combination with the radially polarized light is a great attraction for Raman spectroscopy, fluorescent imaging, particle acceleration, and second harmonic generation [54 and the references therein].

To shed new light on the peculiarities of Bessel beams while concentrating on phase phenomena, we investigate here the field behavior of a submicron-size non-diffracting beam by experimental and theoretical means. We use a highly confined Bessel-Gauss beam that is generated by focusing an annular shaped collimated illumination using a high NA objective. Specifically, the longitudinal phase field of such a beam is investigated to demonstrate the Gouy phase and the emergence of phase singularities. A method developed by Richards and Wolf [55] allows us to calculate the vector light fields near the focus of an aplanatic lens with a high NA. Filtering out the inner NA of the illuminating beam simulates the experimental situations. This allows us to simulate in an elegant way the light propagation in agreement to the experimental situation. Therefore, simulation results can be compared to our measurements.

Generally, the non-diffracting Bessel beam [56] is an exact solution to Maxwell's equations where the radial amplitude distribution corresponds to a Bessel function. The complex field amplitude is denoted as  $\exp(ik_z z) \cdot J_0(k_r r)$ , where  $k_r$  and  $k_z$  are wave vectors in the radial and longitudinal directions, respectively, and  $J_0$  is the zeroth order Bessel function of the first kind. Physically, these beams are slightly pathologic since they are infinitely extended in space, each ring of the Bessel beam carries the same amount of energy which adds up to infinity, the phase among adjacent rings differs exactly by  $\pi$ , and the Fourier spectrum of such Bessel beam is an infinitely thin ring. In other words, perfect Bessel beams are inaccessible in real world experiments but can only be approximated. However, nearly non-diffracting beams, so-called Bessel-Gauss beams [57], with finite power can be realized that propagate over a comparably long distance without significant divergence. This kind of quasi-Bessel beams, whose transverse field distribution imitates the Bessel function and the non-diverging distance is significantly extended compared to that of the focused Gaussian beam, can be generated by using an axicon lens [58, 59], an annular slit at the back focal plane of the focusing lens [56, 59], computer generated holograms [60], and diffraction of Gaussian beam by an opaque disk [61]. Another practical way is to focus an annularly shaped parallel illumination [3, 43, 62]. This method allows an easy adjustment of the beam size along the radial and longitudinal directions by changing the numerical aperture (NA) of the focusing lens. Moreover, the size of the inner blocking disc of the annularly incident beam can be used to vary the amount of the axial phase shift that find important roles in third harmonic generation microscopy and coherent anti-Stokes Raman scattering microscopy [43 and the references therein].

### 4. Experimental and theoretical backgrounds

To study experimentally the complex field distribution in space, we employ a high-resolution interference microscope (HRIM) to measure amplitude and phase in the entire 3D space. Details of the experimental setup are reported elsewhere [63, 64]. Longitudinal-differential (LD) interferometry [40], which is a particular measurement mode of the HRIM, allows to

directly measure the axial phase shift of a beam of interest with reference to a plane wave. All experimental and theoretical investigations were performed at a single wavelength of 642 nm (CrystaLaser: DL640-050-3). The achievable spatial resolution for the amplitude field is subject to the diffraction limit of the observing objective, a 100X/NA0.9 HC PL FLUOTAR from Leica Microsystems. The Richards and Wolf method [55] was employed to rigorously simulate the field distributions near the focus of an NA = 0.9 aplanatic lens in air from a linearly polarized (along the x-axis) plane wave. The computational domain is set to be  $5 \times 5 \times 5 \mu\text{m}^3$  in the xyz-axes. This is sufficiently large and matched the experiments.

The Bessel-Gauss beam is generated by focusing an annular shaped collimated beam, whose inner NA corresponds to 0.72 (half angle =  $45.7^\circ$ ). In practice, an annular central disc blocks approximately 50% of the entrance pupil of the focusing objective (Leica Microsystem, 50X/NA0.9 HXC PL APO) on which a linearly polarized (in the x-axis) collimated beam is incident. In such configuration, the Fourier spectrum at tangential wave vectors smaller than the tangential wave vector corresponding to the inner NA ( $\text{NA} < 0.72$ , i.e.  $< 45.7^\circ$  in air) is blocked and set to zero. As a consequence, the amplitude distribution in the focal plane resembles a zeroth-order Bessel function of the first kind in the radial direction within a finite extent. The focusing causes a Gaussian apodization in the amplitude distribution that can be represented as a product of a Bessel function and a Gaussian profile in real space. Therefore, this type of experimental Bessel beam is known as Bessel-Gauss beam [57, 62].

Figure 1 shows the schematic of the experimental arrangement and the wave vector representation for the angular spectrum of the Bessel beam. The half angle of the inner focal cone  $\theta$  corresponds to the inner NA of the annular illumination. For simplicity, the focused annular beam is illustrated as two parallel beams overlapping near the focal point of the focusing lens. It will be shown that this basic concept of two interfering plane waves properly describes all the phenomena that will be observed. The propagation distance  $z_{\text{prop}}$  is defined to be the axial diagonal of the diamond-shaped overlapping region in Fig. 1(b). The wave vector representation in Fig. 1(c) facilitates the derivation of the Gouy phase using the tilted wave concept from Ref. 43. When a tilted plane wave propagates at a direction that has an angle  $\theta$  with respect to the optical axis, in our case the z-direction, the phase retardation along this axis compared to the on-axis plane wave is given by

$$\Delta\phi = z(k_z - k), \quad (1)$$

with  $z$  as the axial distance, the wave number  $k$ , and the  $z$  component of  $k$  as  $k_z$  in Fig. 1(c). The term containing the difference of wave vectors can be more generally written with respect to the transverse component of  $k_t$  as

$$k_z - k = \sqrt{k^2 - k_t^2} - k. \quad (2)$$

Since Eq. (2) does not yield analytical expression in most cases, certain approximations are required. While Eq. (2) approximates to  $-k_t^2/(2k)$  for the paraxial case, the high NA focusing case (i.e., non-paraxial case) requires higher order approximation and Eq. (2) can be extended up to the second order [43] as

$$\sqrt{k^2 - k_t^2} - k \approx -\frac{k_t^2}{2k} - \frac{k_t^4}{8k^3}. \quad (3)$$

In our scenario the inner NA of 0.72 would usually suggest the consideration of such higher order approximation. However, it will be shown that such higher orders do not need to be taken into account and Eq. (1) will be shown to provide an adequate measure for the Gouy phase of the Bessel beam [37]. We approximate the tilt angle  $\theta$  as the average value of the inner and outer NAs. In our example with  $\text{NA}_{\text{inner}} = 0.72$  and  $\text{NA}_{\text{outer}} = 0.9$ , the angle  $\theta$  equals  $55.1^\circ$ . Using  $k_z = k \cos\theta$  and  $z = z_{\text{prop}}$  Eq. (1) can be re-written as

$$\Delta\phi = z_{prop} k(\cos\theta - 1). \quad (4)$$

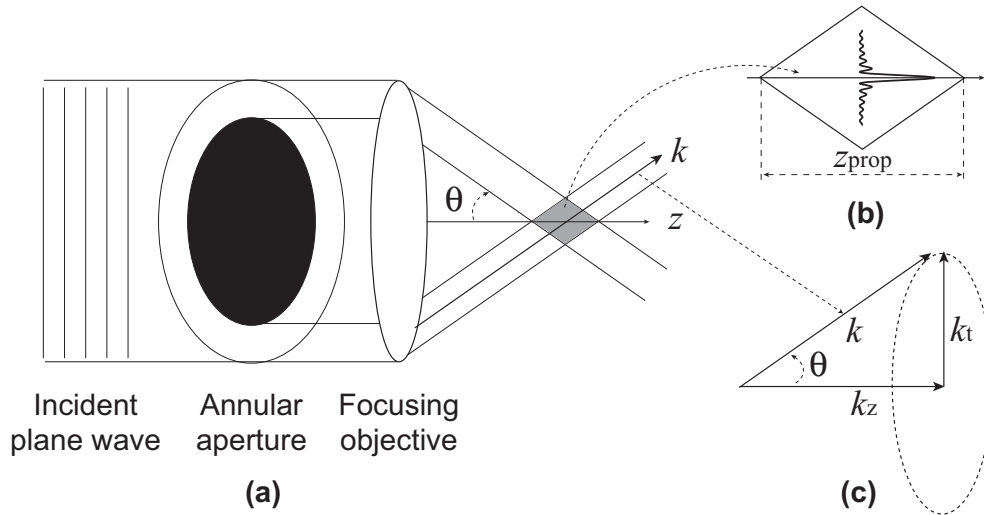


Fig. 1. (a) Schematic of the generation of the Bessel-Gauss beam by focusing the annular shaped collimated incidence. (b) Magnified view of the central spatial domain with a diamond shape: the overlapping region that corresponds to the propagation distance ( $z_{prop}$ ). (c) The wave vector representation of the Bessel beam:  $k$  is the incident wave vector,  $k_z = k\cos\theta$  the longitudinal component of  $k$ , and  $k_t = k\sin\theta$  the transverse component of  $k$ .

## 5. Intensity distributions

The measured and simulated intensity distributions of the generated Bessel-Gauss beam in the  $x$ - $z$  plane are shown in Fig. 2, where the incident light propagates along the positive  $z$ -axis. The high NA focusing leads to a strong confinement of such a non-diffracting beam in all directions. The typical features, such as relatively strong intensity in the side lobes and the elongated focal spot along the  $z$ -axis, are clearly observed in both experiment and simulation. Note that the intensity distribution in the  $x$ - $z$  plane, in general, represents the normalized energy density of the total electric field, i.e.  $|E_t|^2 = |E_x|^2 + |E_y|^2 + |E_z|^2$ . Here,  $E_x$ ,  $E_y$ , and  $E_z$  are the complex electric field components and  $|E_t|^2$  is usually referred to as the total electric field or the field intensity  $I$ . However, Fig. 2(b) shows only  $|E_x|^2$  because  $E_y$  is naturally zero at the  $y = 0$  plane and the longitudinal electric field component  $E_z$  is not measurable with a far-field measurement system, such as conventional optical microscopes. Since the focusing NA is high, rigorous simulations of the vectorial diffraction problem are necessary to provide correct information of light fields near the focus.

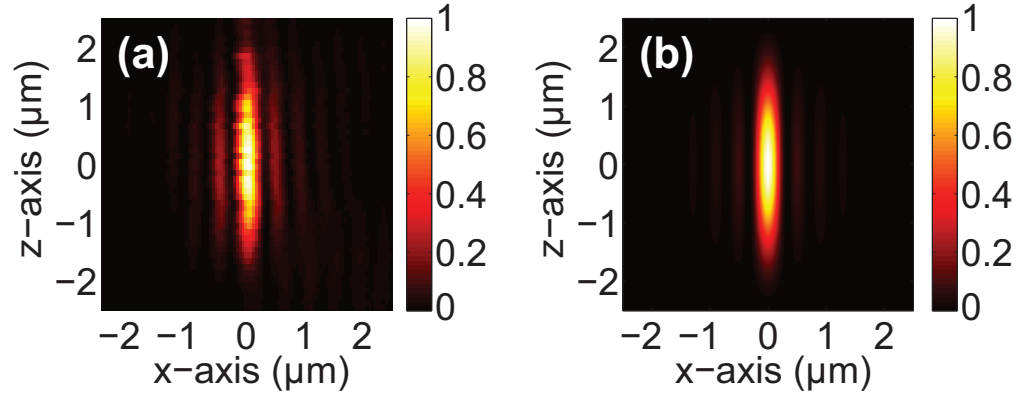


Fig. 2. The measured and simulated amplitude distributions in the  $x$ - $z$  plane: (a) experimental and (b) numerical results (only  $E_x$  is accounted). The intensities are normalized. The image size is  $5 \times 5 \mu\text{m}^2$ .

## 6. Phase distributions

The LD phase mode of the HRIM directly obtains the phase difference between the object wave and a reference plane wave in each measurement plane. The longitudinal slice, crossing the optical axis, of such a phase map is called the LD phase distribution and visualizes directly the phase anomaly. Furthermore, a 2D propagating phase map, which provides a glimpse on the actual phase evolution in space, can be easily reconstructed by wrapping the LD phase with a known value, for instance, the effective wavelength ( $\lambda_{\text{eff}}$ ) along the  $z$ -axis of the tilted wave, which is given as

$$\lambda_{\text{eff}} = \frac{\lambda}{\cos \theta}. \quad (5)$$

Note that this is valid within a simplified 2D ( $x$ - $z$  plane) model of the annular geometry of the angular spectrum of the Bessel-Gauss beam. In our case, the tilt angle of the focal cone  $\theta = 55.1^\circ$  leads to an effective wavelength of approximately  $1.1 \mu\text{m}$ . Due to the abovementioned reasons for non-measurability of  $E_z$  and the vanishing of the  $y$ -component of electric field in the plane of interest, the phase as shown corresponds to the phase of the  $x$  component of the electric field. In general, the Gouy phase of a focused, monochromatic field at an axial point is defined as the difference between the argument (or “phase”) of the object field and that of a referential plane wave of the same frequency [65]. We would like to stress that the term Gouy phase in a strict sense is used to assess the phase evolution of a wave near its focus. There, the Gouy phase describes the deviation of the phase relative to that of a plane wave. Although we investigate here the phase evolution of a Bessel-Gauss beam and discuss its inherent properties along the entire propagation direction and not just in a spatial region that can be understood as the focus, we would like to interpret this here as a Gouy phase for simplicity as well. We understand this as a reasonable nomenclature since, at least for the ideal Bessel beam, a focus cannot be identified since the beam is non-diffracting, i.e., it entirely preserves its shape everywhere in space.

In our study, the difference of the phase of the plane wave from that of the object wave is directly provided by the LD phase distribution. Figure 3(a) shows the measured LD phase distribution of the Bessel-Gauss beam. The propagating phase map is reconstructed by wrapping the LD phase map with  $\lambda_{\text{eff}} = 1.1 \mu\text{m}$  as shown in Fig. 3(b). The planar wavefronts emerging from the left and right hand side corners in the bottom of the Fig. 3(b) perfectly corresponds to the proposed 2D model where two tilted plane waves propagate towards each other. They are characterized by a tangential wave vector component with opposite sign but they do share the same longitudinal wave vector component. Here, the tilt angle of these

planar wavefront is the same ( $55.1^\circ$ ) with respect to the positive  $z$ -axis. When two planar wavefronts overlap, as shown in the diamond shaped region of Fig. 1(b), the resulting field pattern corresponds to that of a two-beam interference pattern. Such a diamond shaped overlapping region can also be found in the measurement in Fig. 3(b).

The results of numerical simulations by the Richards and Wolf method are shown in Figs. 4(a) and 4(b) for the LD phase and the propagating phase, respectively. Note that the natural outcome from the simulation is the propagating phase (i.e. absolute phase) as shown in Fig. 4(b). The LD phase as shown in Fig. 4(a) is reconstructed by subtracting the calculated phase in Fig. 4(b) from the phase of a referential plane wave of the same frequency in each transverse plane. The construction in simulation, therefore, is exactly opposite as in the measurements. Nonetheless, the simulation is in perfect agreement with the experiments, which are shown in Fig. 3.

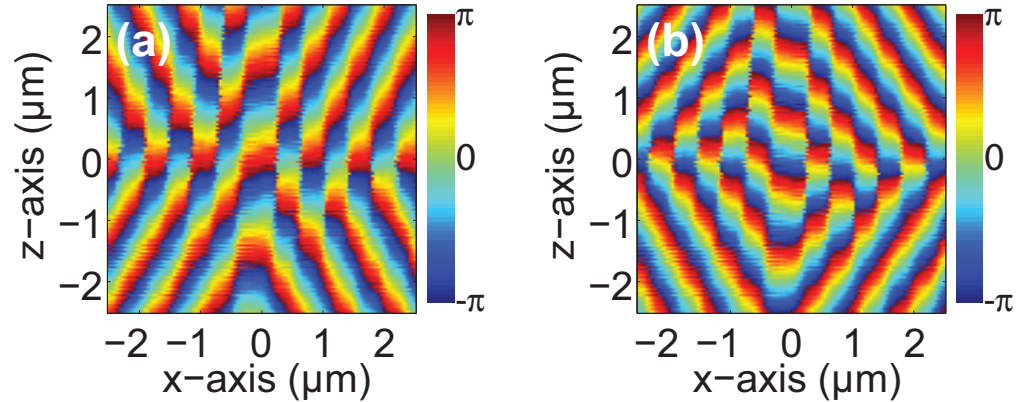


Fig. 3. (Color online) The measured phase distributions in the  $x$ - $z$  plane: (a) the longitudinal-differential phase and (b) the propagating phase. The phase is displayed in radian [from  $-\pi$  to  $\pi$ ]. The image size is  $5 \times 5 \mu\text{m}^2$ .

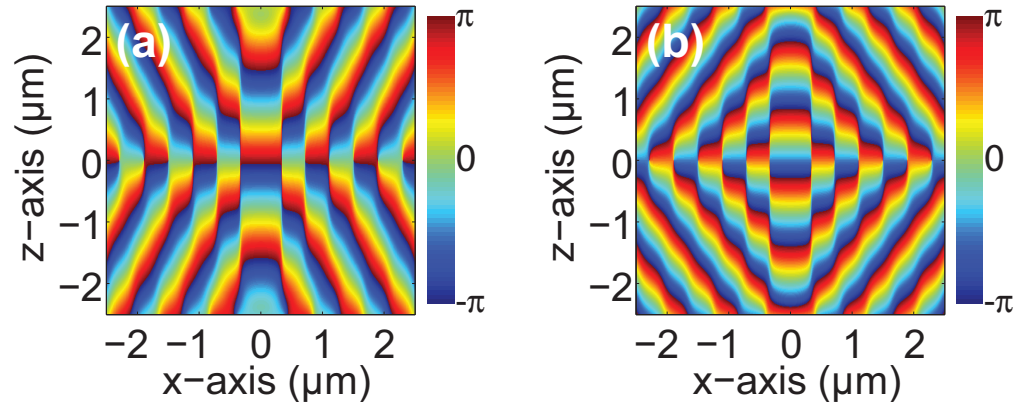


Fig. 4. The simulated phase distributions in the  $x$ - $z$  plane: (a) the longitudinal-differential phase and (b) the propagating phase. The phase is displayed in radian [from  $-\pi$  to  $\pi$ ]. The image size is  $5 \times 5 \mu\text{m}^2$ .

As observed in Figs. 3 and 4, the non-diffracting character of the Bessel beam causes the Gouy phase to grow along the propagation direction [see Eq. (4)]. In other words, the phase anomaly exceeds the ordinary Gouy phase of  $\pi$  and it continues to grow across the spatial domain where the Bessel-Gauss beam possesses a non-diffracting shape, i.e. within the spatial domain that was called the overlap region. In Fig. 3(b), the propagation distance of the non-diffracting Bessel-Gauss beam  $z_{\text{prop}}$  is found to be approximately  $5 \mu\text{m}$ , which corresponds to

the axial diagonal of the diamond-shape region. The on-axis axial phase shift, i.e. the phase anomaly, is calculated to be  $6.7 \pi$  using Eq. (4) with  $\lambda = 642 \text{ nm}$  and  $\theta = 55.1^\circ$ . The experimental result is found by unwrapping the on-axis LD phase profile of Fig. 3(a). We found experimentally a value of  $6.63 \pi$ , being in excellent agreement with the analytical estimation. The derived analytical solution Eq. (4) has been obtained without any higher order approximations as given in Eq. (3) [43]. Therefore, to neglect higher order approximations seems to be justified by the experimental results on both a quantitative and qualitative level.

We further note from Figs. 3 and 4 that in the focused light a phase singularity is located in the dark ring of zero amplitude that surrounds the central bright focal spot [3, 66]. Another consequence of the non-diffracting feature is the propagation of the phase singularity in space along straight trajectories. For the Bessel beam, the transverse field distribution exhibits such dark (i.e. amplitude = 0) rings between the bright intensity lobes. The amplitude node, which is the closest to the optical axis with the longest extend in propagation direction, is less vulnerable against perturbation. This node is located between the central and the 1st side lobe. Since the transverse field distribution does not vary upon propagation, the phase singularity appears in any transverse planes within  $z_{\text{prop}}$ . This phenomenon can be clearly seen in both experiments and simulations, shown in Figs. 3(b) and 4(b), respectively. There, the phase singularities next to both sides of the optical axes follow linear trajectories. In the entire three-dimensional phase distribution in theory the geometry defined by the trajectories of the phase singularities would correspond to an elliptic cylinder which is a consequence of the vectorial nature of light (it would be a circular cylinder for linearly polarized light in the paraxial and scalar approximation). As the amplitude of the side lobes is relatively strong, the phase singularities between each side lobe are also prominently visible.

## 7. Phase anomalies in Bessel-Gauss beam

To quantify the results to an even larger extent, we concentrate on the axial phase not only for the center of the beam (the optical axis) but also for the side lobes. For such non-diffracting beams the on-axis fields within the central lobe are of utmost importance since many applications exploit it. In Fig. 5 we provide a comparison of the on-axis propagating phase profiles obtained from Figs. 3(b) and 4(b): the solid line for the experiment and the dashed line for the simulation. As expected, the larger effective wavelength  $\lambda_{\text{eff}}$  due to the tilt angle  $\theta$  [see Eq. (5)] is clearly visible as the period of the  $2\pi$  modulation and equals approximately  $1.1 \mu\text{m}$ .

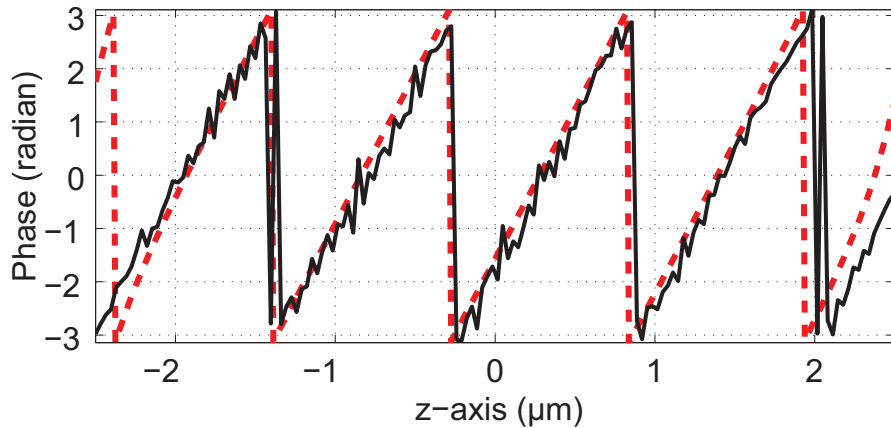


Fig. 5. On-axis phase profiles from Figs. 3(b) and 4(b). The solid line represents the experiment. The dashed line represents the simulation. The period of  $2\pi$  modulation defines the effective wavelength, here  $\lambda_{\text{eff}} = 1.1 \mu\text{m}$  [see Eq. (5)].

The overall axial phase shift is obtained by unwrapping the extracted longitudinal-differential phase data from Figs. 3(a) and 4(a). Since the non-diffracting transverse field

distribution influences fields not only in the central lobe but also in the side lobes, it is interesting to compare the phase anomalies in the central, 1st, and 2nd side lobes. Figure 6 plots the Gouy phase of each lobe obtained from experiment and simulation together with the analytical result. For convenience, the initial axial phase shifts of the central and the 2nd lobes are set to be zero. The solid line represents the analytical result, the dashed lines the simulations, and the markers the experiments. As it can be anticipated by Eq. (4), the anomalous axial phase shift grows linearly with the propagation distance  $z_{\text{prop}}$  and with a factor of  $(\cos\theta - 1)$ . The phase anomaly of each lobe can be calculated by Eq. (4), but the  $\pi$ -jump originating from the phase singularity should be considered for each side lobe separately. While the central lobe and the even number of lobes have exactly the same Gouy phase, the odd number of lobes exhibits a Gouy phase with an offset of  $\pi$  [i.e., the result of Eq. (4) +  $\pi$ ]. This is due to the nature of the Bessel function in the transverse direction, where each lobe has a  $\pi$  phase difference with respect to its neighboring lobe due to the phase singularity. The cylindrical form of the phase singularity separates each bright lobe within in the non-diffracting region as it propagates. The experimental and numerical data for the central, 1st, and 2nd lobes are extracted from Figs. 3(a) and 4(a). The phase anomalies for the central and 2nd lobes are perfectly overlapping with the analytical result. The phase shift for the 1st lobe has the same slope with the  $\pi$  offset as expected. Analytical and numerical calculations show an excellent agreement with our experimental findings.

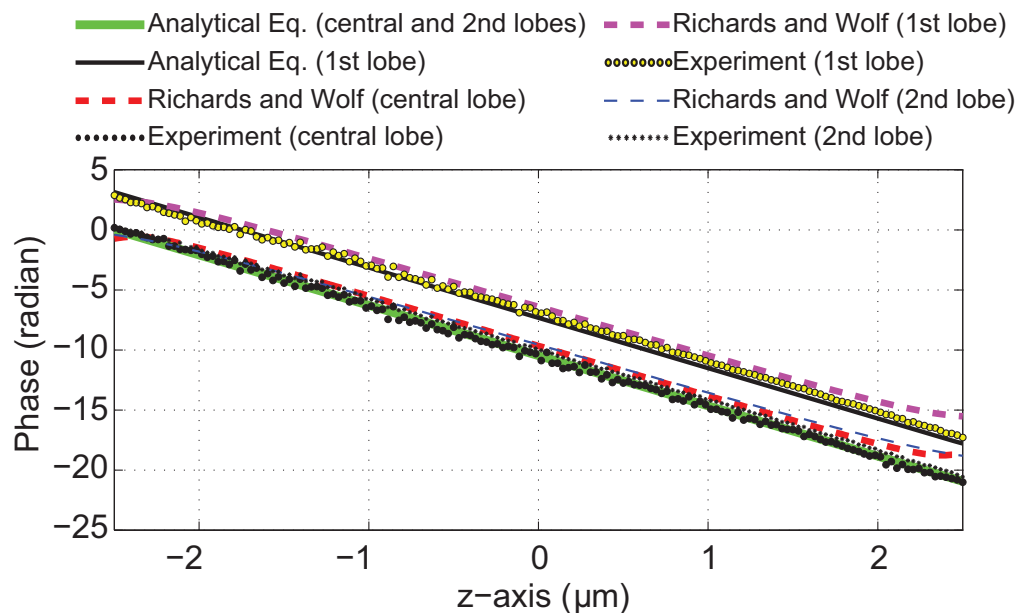


Fig. 6. The overall phase anomalies within the propagation distance ( $z_{\text{prop}}$ ): the solid line represents for the analytical solutions, Eq. (4) for the central and 2nd lobes and its  $\pi$  offset of for the 1st lobe, the dashed lines for the simulations, and the markers for the experiments. Experimental and numerical data are obtained by unwrapping the LD phase profiles from Figs. 3(a) and 4(a). The odd number side lobes have the same Gouy phase with a  $\pi$  offset due to the phase singularity. The initial axial phase shifts for the central and the 2nd lobes are set to be zero for the easy comparison.

The non-diffracting character of Bessel Gauss beams causes two prominent features in the phase distributions. First, the amount of the phase shift continuously grows with respect to the propagation distance and eventually becomes larger than  $\pi$  (i.e. general Gouy phase for a 3D converging wave). Second, the phase singularity that surrounds the central bright spot with a dark ring (i.e. zero amplitude) extends along the entire spatial domain where diffraction is suppressed. Both aspects are shown in the experiments. The rigorous simulations using the

Richards and Wolf method [55] allow verifying the experimental situation by filtering out the inner NA of the annular beam and the numerical results confirm our experimental findings.

## 8. Conclusions

We experimentally and theoretically investigated the Gouy phase anomaly in a Bessel-Gauss beam generated by focusing an annular collimated beam with a high NA objective. The generated beam shows typical features of a Bessel beam, such as relatively strong side lobes and a long propagation distance without a significant divergence. The non-diffracting character makes the Gouy phase to grow proportionally to the propagation distance ( $z_{\text{prop}}$ ) with a factor of  $(\cos\theta - 1)$ . The transverse field distribution does not vary within  $z_{\text{prop}}$  and a phase singularity appears in a cylindrical form. It can be found in the region where the beam does not diverge. The longitudinal-differential phase measurement nicely demonstrates all of the abovementioned phase features of the Bessel-Gauss beam. The numerical simulation using the Richards and Wolf method verifies the measurements and moreover the analytical model [see Eq. (4)]. Such a non-diffracting character influences not only the central lobe but also the side lobes. The growing phase anomalies of each lobe of the Bessel beam up to the 2nd side lobe have been discussed. The Gouy phase of the odd number side lobes is found to have the same amount and slope as the central spot but with an offset of  $\pi$ . Such highly confined Bessel beams are now essential tool for microscopy, meteorology, optical trapping, and micro- and nano-fabrications. Our study provides deeper insight of light fields behavior in such beams.

## Acknowledgment

The research leading to these results has received funding from the Swiss National Science Foundation under Project No. 200021\_125177/1 and the European Community's Seventh Framework Programme FP7-ICT-2007-2 under grant agreement no. 224226.